



Arsenate incorporation in gypsum probed by neutron, X-ray scattering and DFT modeling

Alejandro Fernández-Martínez, Laurent Charlet*

LGIT, University of Grenoble and CNRS, B.P. 53, 38041 - Grenoble Cedex 9, France

Gabriel J. Cuello, Mark R. Johnson

Institut Laue-Langevin, B.P. 156, 38042 Grenoble Cedex 9, France

Gabriela Román-Ross

Departament of Chemistry, University of Girona, Campus de Montilivi, 17071 Girona, Spain

Fabrizio Bardelli

INFM-GILDA c/o ESRF, B.P. 220, 38043 Grenoble Cedex 9, France

Xavier Turrillas

Eduardo Torroja Institute for Construction Sciences, Spanish Council of Scientific Research, Serrano

Galvache 4, 28033 Madrid, Spain

*Corresponding author: Tel: +33 (0)4 76 20 75 71, Fax: +33 (0)4 76 20 76 48, email: fernande@ill.fr

1 The ability of gypsum, a common sulfate mineral, to host arsenic atoms in its crystalline structure, is
2 demonstrated through experimental structural studies of the solid solutions formed upon synthetic co-
3 precipitation of gypsum ($\text{CaSO}_4 \cdot 2\text{H}_2\text{O}$) and arsenic. Neutron and X-ray diffraction methods show an
4 enlargement of the gypsum unit cell proportional to the concentration of arsenic in the solids and to the
5 pH solution value. The substitution of sulfate ions (SO_4^{2-}) by arsenate ions is shown to be more likely
6 under alkaline conditions, where the HAsO_4^{2-} species predominates. A theoretical Density Functional
7 Theory model of the arsenic-doped gypsum structure reproduces the experimental volume expansion.
8 Extended X-ray Absorption Fine Structure (EXAFS) measurements of the local structure around the
9 arsenic atom in the co-precipitated solids confirm solid state substitution and allow some refinement of
10 the local structure, corroborating the theoretical structure found in the simulations. The charge re-
11 distribution within the structure upon substitutions of either the protonated or the unprotonated arsenate
12 species studied by means of Mulliken Population Analyses demonstrates an increase in the covalency in
13 the interaction between Ca^{2+} and AsO_4^{3-} , while the interaction between Ca^{2+} and HAsO_4^{2-} remains
14 predominantly ionic.

18 KEYWORDS: Arsenic, Gypsum, Co-precipitation, Diffraction, EXAFS, DFT Modeling, Arsenate

1 1.- Introduction

2 Arsenic is a metalloid widely distributed in the biosphere and highly toxic [1, 2]. It is present in many
3 industrial sites where mineral ores of lead, copper, zinc, tin, cobalt, gold or silver have been smelted [3].
4 Some As-bearing minerals (like Arsenopyrite FeAsS) are used as raw materials for some of these
5 processes, causing the release of high quantities of arsenic to the environment in the form of arsenite
6 (As^{3+}) or arsenate (As^{5+}) [4, 5]. The toxicity of arsenic depends on its physico-chemical forms, the
7 arsenite species being more mobile and toxic than arsenate. Redox transformations play as well an
8 important role in the arsenic availability to the environment. Changes in the redox state can give rise to
9 precipitation processes of solid phases, thus decreasing the concentration of arsenic in groundwaters [5-
10 7]. The solubility of these solid phases controls the concentration of arsenic aqueous species that are
11 available to the environment. Co-precipitation of As-free minerals like gypsum in the presence of
12 arsenic may lead to long term immobilization of the contaminant, until the host phase is dissolved. For
13 this reason a good understanding of the interactions between the solid and the contaminant and the
14 underlying substitution process is required.

15 The study of ion substitution in minerals has a big impact in the study of the long-term retention of
16 contaminants (as As [6, 8-10], Hg [11], lanthanides [12] or actinides [13, 14]) in polluted environments
17 or potential contaminated sites, as nuclear waste repositories [15]. Substitution processes of arsenic on
18 the calcite surface [16] and into its bulk [8-10] have been recently reported. Substitutions of divalent
19 cations as Co^{2+} , Zn^{2+} , Mn^{2+} , Ni^{2+} or UO_2^{2+} and trivalent cations such as Cm^{3+} or Am^{3+} in calcite have
20 been largely studied by bulk sensitive techniques as X-ray Absorption Spectroscopy (XAS), X-ray
21 Standing Waves, Electron Paramagnetic Resonance (EPR), Neutron Diffraction and Time Resolved
22 Laser Fluorescence Spectroscopy methods [13, 14, 17-22].

23 Gypsum is a common industrial by-product from a number of processes involving neutralization of
24 sulfuric acid and SO_2 -rich fumes [23, 24]. Some industrial activities where mineral ores are smelted
25 generate As-rich gypsum sludges, produced upon neutralization of As-rich acidic solutions. Quite often
26 gypsum from those sludges appears associated to Ca arsenates [4]. However, little is known about

1 arsenic incorporation into the bulk of gypsum, which may potentially lead to its long term
2 immobilization into the mineral structure.

3 Incorporation of anions into the structure of sulfate minerals has been little studied. Paktunc and
4 Dutrizac have demonstrated the ability of jarosite, a sulfate mineral, to host arsenate anions by
5 substitution for sulfate [25]. Fernández-González *et al.* have studied the incorporation of selenate anions
6 SeO_4^{2-} into the sulfate site of gypsum, revealing the complete miscibility diagram for sulfate / selenate
7 substitutions [26]. The arsenate ion, with C_2 tetrahedral symmetry, has a very similar geometry to
8 sulfate, with T_d symmetry, thus opening the hypothesis of an arsenate for sulfate substitution in the bulk
9 of gypsum.

10 In this paper we present the results of a crystallographic study of synthetic gypsum co-precipitated
11 with arsenic at different concentrations and pH values. Solid phases have been studied by neutron and
12 X-ray diffraction experiments. X-ray absorption spectroscopy experiments reveal the local structure of
13 the arsenate ions within the gypsum crystallographic structure. Density Functional Theory (DFT)
14 modeling of the pure and the arsenic-doped gypsum structures help us to understand the mechanisms of
15 substitution of arsenate for sulfate and to elucidate how the charge is redistributed upon the substitution
16 takes place. Finally, Mulliken Population Analyses allow quantifying the changes in the electrostatic
17 interactions between ions for the different protonated / unprotonated species of arsenate.

19 **2.- Materials and Methods**

20 **2.1.- Experimental methods**

21 Gypsum was precipitated from supersaturated solutions of calcium sulfate prepared by mixing
22 directly into a reactor two equimolar aqueous solutions (0.5 M) of reagent-grade CaCl_2 and Na_2SO_4 .
23 The solutions were mixed under stirring to avoid the formation of local precipitates and the temperature
24 was kept at 25°C in a thermostatic water bath. Ten runs were conducted to produce samples at three
25 different total arsenic concentrations and at three different pH values (4, 7.5 and 9), together with a pure
26 gypsum reference sample (see Table 1 for sample description). Sodium arsenate dibasic heptahydrate

1 (Na₂HAsO₄·7H₂O) from Sigma Aldrich® was used as the arsenate source in all the solutions. The pH
2 values were recorded continually as a function of time during syntheses. Final solid arsenic
3 concentrations in the solids were determined by Inductively Coupled Plasma Atomic Emission
4 Spectrometry (ICP-AES) after dissolution in a 10 M HNO₃ solution (Table 1).

5 Powder samples were analysed by neutron diffraction at the high flux powder diffractometer D20 at
6 the Institut Laue-Langevin (ILL), and by X-ray diffraction at the ID11 Materials Science Beamline at
7 the European Synchrotron Radiation Facility (ESRF), in Grenoble (France). Details of the experimental
8 setup have been published elsewhere [14]. The neutron and X-ray diffraction data were analysed by
9 means of Rietveld analysis, using the FullProf software [27]. For neutron refinements a pseudo-Voigt
10 function convoluted with an axial divergence asymmetry function was used to fit the shape of the peaks
11 in order to correct for the large peak asymmetry at low diffraction angle. For the refinement of X-ray
12 data a pseudo-Voigt function was used. Preferred orientation effects [28] affecting the intensity of the
13 (010) reflection of the gypsum structure were considered in the refinements. The Rietveld refinement of
14 the pure gypsum structure was carried out assuming a monoclinic unit cell with *C* 2/*c* space group (no.
15 15) as starting model. The refined atomic parameters are given in Table 2, and compared with other
16 published structures [29, 30]. The refinements of the As-doped gypsum structures have been done by
17 assuming the 4e Wyckoff sulfur position shared with the arsenic atom.

18 EXAFS spectra have been acquired on the BM8-GILDA beamline at the ESRF in Grenoble (France)
19 [31]. All the spectra have been measured at the arsenic K-edge (11867 eV) using a couple of Si (311)
20 monochromator crystals. All the measurements have been performed at 77 K in order to reduce the
21 thermal dumping of the signal.

22 The DFT optimizations of the arsenic-doped gypsum structure allow us to have a model for the local
23 environment of the arsenic atom in the gypsum structure. We use this model as a starting point to
24 calculate the amplitude and back-scattering functions with the FEFF8 code [32]. The coordination for
25 each shell has been fixed to its ideal value, obtained from the DFT models, in order to reduce the
26 correlation between free parameters in the minimization procedure, which were mainly the bond

1 distances and the Debye-Waller factors. The latter take into account both dynamic (thermal induced)
2 and static structural (if present) disorder. Other free parameters were the experimental energy shift and
3 the EXAFS many-body loss factor (S_0^2). The data have been extracted using standard procedures [33].
4 The fits were performed using the MINUIT library from CERN [34].

6 ***2.1.- Theoretical Calculations***

7 Geometrical optimisations of the gypsum unit cell and of $2 \times 1 \times 2$, $2 \times 1 \times 3$ and $3 \times 1 \times 3$ supercells¹ have
8 been performed using the Vienna Ab-initio Simulation Package (VASP) [35]. The calculations were
9 performed at the Gamma point ($k = 0$), using projector augmented wave (PAW) pseudopotentials [36]
10 with a plane wave cutoff of 209 eV and the Perdew–Burke–Ernzerhof (PBE) functional of the
11 Generalized Gradient Approximation (GGA). The residual external pressure (Pulay stress) at end of the
12 relaxations was always equal to zero, so any extra compensation for the Pulay stress was required. The
13 goal was to reproduce the expansion of the unit cell induced by the substitution of arsenic atoms within
14 the gypsum structure. One unit cell of the structure of pure gypsum obtained from Rietveld refinements
15 was used as starting point for all the models (see Figure 1 for a model gypsum unit cell). The volume
16 expansion induced by either the protonated HAsO_4^{2-} or the unprotonated AsO_4^{3-} species was checked in
17 single cells by replacing the four sulfate anions SO_4^{2-} until the replacement of all the sulfur atoms within
18 the unit cell. The same kind of simulation was done with supercells of $2 \times 1 \times 2$, $2 \times 1 \times 3$ and $3 \times 1 \times 3$ in
19 order to reach lower arsenic concentrations in the models. Relative volume variations are used to
20 quantify the amount of arsenic in the gypsum cells. This allows us to avoid in the calculated unit cells of
21 gypsum the effect of shrinkage due to the fact that the optimizations of the geometry are done at zero
22 Kelvin [37].

23 The replacement of sulfate groups by arsenate groups implies not only structural changes in the
24 volume of the gypsum unit cell but also modifications in the electronic charge distribution, which affect
25 the strength of the electrostatic interactions within the cells. Mulliken population analyses [38, 39]

1 (MPAs) have been performed in order to study these charge redistribution processes within the doped
2 and pure gypsum structures. These calculations project into Linear Combinations of Atomic Orbitals
3 (LCAOs) the charge density, thus obtaining values for atomic charges and bond populations [39]. For
4 this reason it is generally acknowledged that population analyses give only semiquantitative
5 information, as they are extremely sensitive to the atomic basis set used. However, relative variations of
6 charge and bond populations of pure and doped models can be used to understand the underlying charge
7 redistribution processes [40-42].

8 For all the MPAs calculations we used a commercial version of the plane wave pseudopotential code
9 CASTEP [43], as implemented in Materials Studio (Accelrys Inc.). Mulliken charges and bond
10 populations are calculated according to the formalism described by Segall et al. [40]. MPAs have been
11 performed on the cell models of the pure and doped gypsum structures that were optimised with VASP.
12 Energy minimisations with fixed atomic positions have been performed using the VASP optimised
13 structures prior to the calculation of the MPAs.

14 For the energy minimisations with CASTEP we used the PBE variation of the GGA [44]. We used
15 ultrasoft pseudopotentials, [45] with a maximum cutoff energy of the plane waves of 340 eV. Another
16 parameter which determines the quality of the calculations is the density of points with which the
17 Brillouin zone is sampled; we used a parameter such that the distances between grid points are less than
18 0.15 \AA^{-1} , comparable to the sampling used for the VASP calculations. Different values for the energy
19 cutoff and different exchange functionals were checked in a first step in order to optimise the
20 convergence of the calculations. The values of the Mulliken charges and bond populations have been
21 shown to converge within the 5% of their value.

22 23 **3.- Results and discussion**

24 ***3.1.- Volume expansion and local environment of arsenic***

25 *Diffraction results*

¹ $l \times m \times n$ representing a supercell of $l \times m \times n$ cells in directions a , b and c , respectively.

1 The neutron and X-ray diffraction patterns (Figures 2 and 3) show the existence of a solid phase with
2 the structure of gypsum and of some other precipitates which cannot be identified within the Inorganic
3 Crystal Structure Database (ICSD) [46]. The Rietveld refinement of the atomic parameters of pure
4 gypsum reveal a very well crystallized phase, as compared to other published structures (Table 2).

5 Only one out of ten of the arsenic-containing samples presents an important weight of other
6 crystalline phase: the sample Y11 shows diffraction peaks of sodium chloride (NaCl) in its X-ray
7 diffraction pattern (Figure 2). A poorly crystallized phase of an unknown precipitate is also found in this
8 sample: the characteristic amorphous halo can be easily seen (Figure 2). These phases are not observed
9 in the neutron diffraction patterns. This reflects the different sensitivity of the methods: X-rays are more
10 sensitive to phases adsorbed on the surface while neutrons probe the bulk of the samples. In the neutron
11 diffraction pattern of sample Y11 (Figure 3) the contribution from the vanadium sample-holder can be
12 distinguished. This is due to the fact that only a small volume of sample was available for the
13 experiment. Therefore, a phase of vanadium was introduced in all the analyses of the neutron data. In
14 the Rietveld refinements of the gypsum phase, the (4e) Wyckoff position corresponding to the sulfur
15 atom has been shared with the arsenic atom, under the hypothesis that arsenate for sulfate substitution
16 occurs. The lattice parameters of the phase of gypsum obtained from combined Rietveld refinements of
17 neutron and X-ray data are shown in Table 3 together with the R-Bragg (RB) and χ^2 values of the fits.

18 A plot of this data set (Figure 4) gives a better understanding of the results. It shows an expansion of
19 the unit cell proportional to the initial arsenic concentration in the solutions, and which slope is strongly
20 dependent on the equilibrium pH value. The biggest expansion is found in samples synthesized at pH 9
21 indicating a preference of the unit cell of gypsum to host protonated arsenate ions HAsO_4^{2-} ($\text{pK}_2 = 7.08$,
22 $\text{pK}_3 = 11.5$) [47]. This result is in agreement with the results expected under the hypothesis of a charge
23 balanced replacement. The charge developed by the arsenate species at different pH values is shown in
24 Table 1 [47].

25 Modeling results

1 Simulations help us to understand the volume expansion. Gypsum cells with both the protonated and
2 unprotonated arsenates were simulated separately. Models of four single cells with one to four arsenate
3 ions each (giving arsenic concentrations of 940, 1809, 3357 and 4696 mM/kg) and four supercells were
4 simulated: two $2 \times 1 \times 2$ supercells with one (358 mM/kg) and two (705 mM/kg) As atoms, and supercells
5 of $2 \times 1 \times 3$ (240 mM/kg) and $3 \times 1 \times 3$ (160 mM/kg) with one arsenic atom each. Same size supercells of
6 pure gypsum have been simulated as well. The obtained cell parameters differ by less than 3% from the
7 experimental ones.

8 The simulations show an expansion of the unit cell volume proportional to the number of sulfate ions
9 that have been substituted by arsenates, following a linear Vegard's law behaviour (Figure 5). It is
10 important to note that the same volume expansion is found for substitutions of protonated and
11 unprotonated arsenate for sulfates.

12 The crystalline structure of gypsum has (010) planes where Ca^{2+} and SO_4^{2-} ions interact through ionic
13 bonding. These planes are held together by H-bonds through water molecules that sit in between them.
14 The S-O bond distance within a sulfate group in the gypsum structure is 1.47 Å [48]. The As-O bond
15 length is roughly 1.69 Å [49], increasing up to 1.79 Å when an H atom is bound to an O in the
16 protonated species. Due to the higher volume of the arsenate ion with respect to the sulfate, the
17 degeneracy of the two X-Ca interatomic distances, that is 2-fold in the pure gypsum structure (X=S), is
18 broken, giving 4 different X-Ca distances in the arsenic-doped gypsum (X=As), as indicated in Table 4.
19 This induces an increase of the lattice parameters a and c . The inter-planar distance between hydrogen-
20 bonded planes expands as well, increasing the lattice parameter b . These changes in the structure result
21 in a volume expansion of the crystal lattice of arsenic-doped gypsum, as indicated in Figure 5.

22 The models allow us to extrapolate the arsenic concentration in the bulk of the samples by comparing
23 the relative volume variations between the experimental and simulated data. The experimental values of
24 the volume expansion have been interpolated in the linear fit that describes the model expansion of the
25 volume (inset Figure 5), giving maximum values for the concentration of arsenic incorporated in the

1 crystallographic structure of gypsum. These concentrations (Table 7) are smaller than the total
2 concentration of arsenic found in the samples (adsorbed and substituted).

3 EXAFS results

4 EXAFS is used to study the immediate atomic environment around a selected absorber atom (up to no
5 more than 10 Å) without requiring long range order of the lattice (a requirement for diffraction
6 techniques). For these reasons, EXAFS is a genuine local and selective probe which can provide
7 complementary information on the lattice structure with respect to diffraction techniques.

8 The k-weighted EXAFS oscillations and the fit curves for the samples Y6, Y8, Y11 are shown in
9 Figure 6. The obtained absorber-backscatterer distances are shown in Table 5 and show a good
10 agreement with the modelled structure. The three samples show little difference in the local atomic
11 environment: the first shell is formed by oxygen atoms in tetrahedral coordination (four-fold
12 degenerated) at a distance of $d_{\text{As-O}} = 1.69 \text{ \AA}$. One of the four As-O distances is 1.79 Å in the theoretical
13 model of the HAsO_4^{2-} ion, which is impossible to distinguish due to the limited resolution of our
14 experimental conditions. The second shell signal originates from the As-Ca bonds which are split in
15 three singly degenerate distances: $d_{\text{AsCa1}} = 3.15 \text{ \AA}$, $d_{\text{As-Ca2}} = 3.31 \text{ \AA}$ and $d_{\text{As-Ca3}} = 3.70 \text{ \AA}$. Contributions
16 from higher coordination shells fall under the detectable threshold. The results are in good agreement
17 with the scenario of replacement of HAsO_4^{2-} for SO_4^{2-} . The As-Ca distances calculated with the DFT
18 modeling agree with experimental values within error bars (Table 5).

20 **3.2.- Charge balance**

21 Charge balance is a strict requirement for any equilibrated substitution that may occur in ion exchange
22 processes. However, the nature of the balancing mechanism can be local or global. Recently, some
23 authors have demonstrated experimentally that the arsenite molecule (AsO_3^{3-}) replaces carbonate
24 molecules in the calcite structure, which results in a non-balanced local charge [20]. In the same way,
25 other authors hypothesize that the charge balance of uranyl ions incorporated in calcite through a non-
26 local mechanism by which Na^+ cations would be compensating the charge [22]. In the case of gypsum,

1 the existence of a 'water interlayer' in the structure (see Figure 1) provides mechanisms for charge
2 balancing, if sulfate is being substituted by the unprotonated AsO_4^{3-} species: formation of H_3O^+
3 molecules is a valid hypothesis that would make the unprotonated arsenate by sulfate substitution hence
4 possible. Other possibilities could include the existence of defects or interstitials, as the inclusion of
5 extra Ca^{2+} cations in the ionic layer. However, our EXAFS data fits very well with the calculated model
6 for the inclusion of the protonated HAsO_4^{2-} , reproducing accurately the distances found in the simulated
7 models. Thus, the existence of a local charge balance mechanism is corroborated experimentally with a
8 local probe (EXAFS). In this context, the electrostatic effects of a local substitution mechanism
9 (HAsO_4^{2-}) and of a non-local substitution mechanism (AsO_4^{3-}) will be shown.

10 Under oxidizing conditions and at pH higher than $\text{pK}_2=11.5$, unprotonated arsenate (AsO_4^{3-}) becomes
11 the aqueous arsenic dominant species. Unprotonated arsenate is an ion with C_2 tetrahedral symmetry
12 very similar to sulfate ions (SO_4^{2-}), with T_d symmetry. From the point of view of symmetry, the very
13 similar geometry of both ions would suggest that the replacement is more likely under very alkaline
14 conditions (i.e., at pH higher than 11), where AsO_4^{3-} is thermodynamically the more stable species. The
15 fact that the same volume expansion is found for both AsO_4^{3-} and HAsO_4^{2-} implies that any assumption
16 of which species is responsible for the volume expansion cannot be made *a priori*. In the protonated
17 HAsO_4^{2-} , species of lower symmetry than AsO_4^{3-} , the As-O bond length is increased for the O atom
18 bonded to the H atom.

19 In order to evaluate the strength of electrostatic interactions within the gypsum structure and their
20 changes when a sulfate ion is substituted by an arsenate, we have performed MPAs in the pure and
21 doped structures of gypsum. As stated above, the gypsum structure is formed by planes of ionic bonded
22 Ca^{2+} and SO_4^{2-} ion pairs; these planes are hold together by H-bonds through water molecules located in
23 between the planes (view Figure 1). When an arsenate ion substitutes a sulfate, the degree of ionicity of
24 both the Ca^{2+} and the anions is changed, and the aim of these analyses is to quantify these changes.

25 This kind of analysis gives values for the charge by integrating into LCAOs the charge density
26 distribution which results from the energy optimization of the DFT calculation. Different values for the

1 charges are assigned to each atom, as well as values for the bond populations and its bonding or
2 antibonding character.

3 The ionicities of the Ca^{2+} cations and of the AsO_4^{3-} , HAsO_4^{2-} and SO_4^{2-} ions in the structure of
4 gypsum have been evaluated by calculating their effective ionic valence, which has been defined as the
5 difference between the formal ionic charge and the Mulliken charge of the ion species in the crystal
6 [41]. In the case of an ideal ionic bond the effective ionic valence has a null value, while values greater
7 than zero indicate increasing levels of covalency. We have evaluated the Mulliken charges for all the
8 atoms and the bond populations for the bonds with lengths up to 3.5 Å in all the three different models:
9 pure gypsum, HAsO_4^{2-} doped gypsum and AsO_4^{3-} doped gypsum. The effective ionic charges have been
10 calculated considering a formal valence of +2 for the Ca^{2+} , SO_4^{2-} and HAsO_4^{2-} ions (without considering
11 the charge of the H atom in the latter), and a formal charge of +3 for the AsO_4^{3-} ion.

12 Results are shown on Tables 5 and 6, together with the spilling parameter of each of the calculations.
13 This parameter indicates the percentage of valence charge that has been missed in the projection. A low
14 spilling parameter indicates a good representation of the electronic bands using the LCAO basis set.
15 The effective ionic valence for the four Ca^{2+} cations (see Figure 7) in pure gypsum is $0.58 e^-$. The
16 HAsO_4^{2-} doped gypsum has values for the Ca^{2+} effective ionic valence that range from $0.59 e^-$ to $0.63 e^-$.
17 The Ca^{2+} cations in the AsO_4^{3-} doped gypsum have values of $0.70 e^-$ and $0.63 e^-$.

18 The degree of covalency can also be evaluated through the bond populations. Results are shown in
19 Table 6, and can be summarised in two points:

20 1) The values for the Ca-O bond populations in the AsO_4^{3-} doped gypsum are higher than in the other
21 two structures. The Ca-O bond population in the pure gypsum has a mean value of $0.07 e^-$, exactly equal
22 to that of the HAsO_4^{2-} doped gypsum, while the mean value in the AsO_4^{3-} doped gypsum is $0.095 e^-$.

23 2) The bond population of the Ca-S or Ca-As bonds are $-0.20 e^-$ in the pure gypsum (negative value
24 meaning that the antibonding orbital is populated), $-0.35 e^-$ in the HAsO_4^{2-} doped gypsum and $-0.73 e^-$ in
25 the AsO_4^{3-} doped gypsum.

1 These results can be interpreted in terms of a redistribution of the extra valence electron introduced
2 with the AsO_4^{3-} ion over its neighbours. They reflect an increase of the covalency in the $\text{Ca}^{2+} - \text{AsO}_4^{3-}$
3 interaction. In the HAsO_4^{2-} ion the H atom acts as a charge 'reservoir' for this electron, thus not
4 allowing the extra electron to spread over its neighbours. This results in a higher degree of ionicity in
5 the $\text{Ca}^{2+} - \text{HAsO}_4^{2-}$ interaction, similar to the $\text{Ca}^{2+} - \text{SO}_4^{2-}$ ionicity in pure gypsum structure.

6 The mean Ca-O, Ca-As and Ca-S interatomic distances are presented in Table 6. The higher volume
7 of the arsenate ion with respect to the sulfate is reflected in the shortening of these distances. In
8 principle, a shorter distance would give rise to an increase of the covalency, as the overlap between the
9 orbitals would be higher. However, the results of these analyses show that this is not the case for the
10 HAsO_4^{2-} ion. The effective ionic valence of its atoms and the bond population values are very similar to
11 the values of the pure gypsum structure. Hence, low incorporation of AsO_4^{3-} molecules can be expected
12 in the absence of any non-local mechanism of charge balancing (interstitials...).

13 14 **Conclusions**

15 The ability of arsenate to isomorphically substitute for sulfate in the gypsum structure is demonstrated
16 in the present study by measuring the volume expansion of the unit cell with neutron and x-ray
17 diffraction techniques. This volume expansion has been found to increase with the equilibrium pH
18 value, up to pH 9. This is in agreement with the evolution of the concentration of HAsO_4^{2-} ions in
19 solution. At pH 4 only a very low percentage of the arsenates are protonated, H_2AsO_4^- being the
20 dominant species. As pH increases HAsO_4^{2-} becomes the dominant species, thus giving rise to a higher
21 rate of isomorphic substitution within gypsum.

22 Simulations allow us to reproduce the expansion of the volume of the unit cell as arsenic is
23 increasingly substituted for sulfur. A similar expansion is found for both the HAsO_4^{2-} and the AsO_4^{3-}
24 doped gypsum structures, indicating that the extra proton introduced in HAsO_4^{2-} does not have any
25 influence on the volume of the ion itself. However, MPAs show the influence of the H atom as an
26 electron reservoir that makes the substitution of arsenic (pentavalent) for sulfur (tetravalent) possible.

1 The values of the theoretical expansion of the volume help us to make an estimation of the total amount
2 of arsenic that can be hosted into the bulk of gypsum in ideal conditions (Table 7).

3 The local structure of the arsenic atom in the bulk of gypsum has been probed by XAS. Two different
4 shells can be distinguished: one formed by four oxygen atoms, constituting the arsenate ion, and a
5 second shell formed by calcium atoms placed at three different distances. These distances coincide
6 within the experimental error with the distances of the DFT optimized structure of HAsO_4^{2-} doped
7 gypsum.

8 The MPAs have helped us to understand how the charge is redistributed upon substitution, and to
9 elucidate what would happen if this substitution took place at a higher pH value, where the AsO_4^{3-}
10 species is the most stable. The models show that the protonated arsenate species is introduced in the
11 gypsum structure conserving the degree of ionicity of the ion pairs $\text{Ca}^{2+} - \text{SO}_4^{2-}$. The extra proton acts as
12 a charge reservoir for the extra electron introduced within the HAsO_4^{2-} ion. This is not the case for the
13 $\text{Ca}^{2+} - \text{AsO}_4^{3-}$ interactions, where the ionicity is reduced, making the substitution process less likely.
14 Recently, some experimental results of EPR measurements on another ionic mineral, namely natural
15 calcite [22] have demonstrated the ability of calcite to host As atoms in its bulk through a similar
16 substitution mechanism (arsenite AsO_3^{3-} for carbonate CO_3^{2-}), in which the charge is not balanced, at
17 least at a local (few Angstroms) scale. Even though direct observation of the local structure of the
18 arsenic atom in calcite has to our knowledge not yet been published, we think that a modeling approach
19 could help to understand the effect of this mechanism of substitution on the electrostatic interactions
20 within the calcite structure.

21 Our results support the hypothesis of arsenic immobilisation by incorporation into the bulk of
22 gypsum. When a hazardous ion like arsenate is incorporated into the bulk of a mineral, it can be
23 considered immobilised, reducing its mobility and the potential risk of environmental contamination.
24 Quantifying the exact concentration of arsenic that can be hosted into the gypsum structure can help to
25 improve the knowledge on the long term stability of contaminated sludges and has important
26 consequences for site remediation actions.

Acknowledgements

The authors thank Dr. Gavin Vaughan and Dr. Javier Campo for their assistance in the diffraction experiments, the Italian CRG GILDA and ID11 (Experiment ME-171) beamlines at the ESRF and the ILL (Experiment 5-25-57) for the allocation of the beamtime. Contributions from three anonymous reviewers are kindly acknowledged. This work was partially supported by the Action ECOS-SUDA02U01 and EC2CO CNRS program.

References

- (1) Nriagu, J. O. *Arsenic in the Environment. Part I: Cycling and Characterization*; Wiley Series in Advances in Environmental Science and Technology, Volume 26, 1994.
- (2) Smedley, P. L.; Kinniburgh, D. G. *Appl. Geochem.* **2002**, *12*, 517.
- (3) Juillot, F.; Ildefonse, P. H.; Morin, G.; Calas, G.; De Kersabiec, A. M.; Benedetti, M. *Appl. Geochem.* **1999**, *14*, 1031.
- (4) Charlet, L.; Ansari, A. A.; Lespagnol, G.; Musso, M. *Sci. Tot. Env.* **2001**, *277*, 133.
- (5) Sadiq, M. *Wat., Air & Soil Pollut.* **1995**, *93*, 117.
- (6) Morin, G.; Juillot, F.; Casiot, C.; Bruneel, O.; Personne, J.-C.; Elbaz-Poulichet, F.; Leblanc, M.; Ildefonse, P.; Calas, G. *Environ. Sci. Technol.* **2003**, *37*, 1705.
- (7) Tournassat, C.; Charlet, L.; Bosbach, D.; Manceau, A. *Environ. Sci Technol.* **2002**, *36*, 493.
- (8) Román-Ross, G.; Charlet, L.; Cuello, G. J.; Tisserand, D. *J. Phys. IV.* **2003**, *107*, 1153.
- (9) Fernández-Martínez, A.; Román-Ross, G.; Cuello, G. J.; Turrillas, X.; Charlet, L.; Johnson, M. R.; Bardelli, F. *Phys. B.* **2006**, *385-386*, 935.
- (10) Román-Ross, G.; Cuello, G. J.; Turrillas, X.; Fernández-Martínez, A.; Charlet, L. *Chem. Geol.* **2006**, *233*, 328.

- 1 (11) Sobolev, O.; Cuello, G. J.; Román-Ross, G.; Skipper, N. T.; Charlet, L. *J. Phys. Chem. A.*
2 **2007**, *111*, 5123.
- 3 (12) Pitteloud, C.; Powell, D. H.; González, M. A.; Cuello, G. J. *Coll. Surf. A.* **2003**, *217*, 129.
- 4 (13) Stumpf, T.; Fernandes, M. M.; Walther, C.; Dardenne, K.; Fanghanel, T. *J. Coll. Inter.*
5 *Sci.* **2006**, *302*, 240.
- 6 (14) Fernandes, M. M. ; Stumpf, T. ; Rabung, T. ; Bosbach, D. ; Bauer, A.; Fanghanel, T.
7 *Geochim. Cosmo. Acta.* **2004**, *68*, A85.
- 8 (15) *Dossier 2005 Argile. Référentiel du comportement des radionucléides et des toxiques*
9 *chimiques d'un stockage dans le Callovo-Oxfordien jusqu'à l'homme.* ANDRA, 2005..
- 10 (16) Cheng, L. W. ; Fenter, P. ; Sturchio, N. C.; Zhong, Z.; Bedzyk, M. J. *Geochim. Cosmo.*
11 *Acta.* **1999**, *63*, 3153.
- 12 (17) Lamble, G. M.; Reeder, R. J.; Northrup, P. A. *J. Phys. IV.* **1997**, *7*, 793.
- 13 (18) Cheng, L.; Sturchio, N. C.; Woicik, J. C.; Kemner, K. M.; Lyman, P. F.; Bedzyk, M. J.
14 *Surf. Sci.* **1998**, *415*, 976
- 15 (19) Cheng, L.; Sturchio, N. C.; Bedzyk, M. J. *Phys. Rev. B.* **2000**, *61*, 4877.
- 16 (20) Di Benedetto, F.; Costagliola, P.; Benvenuti, M.; Lattanzi, P.; Romanelli, M.; Tanelli, G.
17 *Earth Plan. Sci. Lett.* **2006**, *246*, 458.
- 18 (21) Sturchio, N. C.; Antonio, M. R.; Soderholm, L.; Sutton, S. R.; Brannon, J. C. *Science.*
19 **1998**, *281*, 971.
- 20 (22) Kelly, D. D.; Newville, M. G.; Cheng, L.; Kemner, K. M.; Sutton, S. R.; Fenter, P.;
21 Sturchio, N. C.; Spötl, C. *Environ. Sci. Technol.* **2003**, *37*, 1284.
- 22 (23) *Active and Semi-Passive Lime Treatment of Acid Mine Drainage.* United States
23 Environmental Protection Agency, May 2006.

- 1 (24) Gominšek, T.; Lubej, A.; Pohar, C. *J. Chem. Techn. & Biotech.* **2005**, *80*, 939.
- 2 (25) Paktunc, D.; Dutrizac, J. E. *Can. Min.* **2003**, *41*, 905.
- 3 (26) Fernández-González, A.; Andara, A.; Alía, J. M.; Prieto, M. *Chem. Geol.* **2006**, *225*, 256.
- 4 (27) Rodríguez-Carvajal, J. *Collected Abstracts of Powder Diffraction meeting*. Ed. By J.
5 Galy. Toulouse, France. 1990.
- 6 (28) Grattan-Bellew, P. E. *Am. Min.* **1975**, *60*, 1127.
- 7 (29) De la Torre, A. G.; López-Olmo, M. G.; Álvarez-Rúa, C.; García-Granda, S.; Aranda, M.
8 *A. G. Pow. Diff.* **2004**, *19*, 240.
- 9 (30) Schofield, P. F.; Knight, K. S.; Stretton, I. C. *Am. Min.* **1996**, *81*, 847.
- 10 (31) Pascarelli, S.; Boscherini, F.; D'Acapito, F.; Hrdy, J.; Meneghini, C.; Mobilio, S. *J.*
11 *Synch. Rad.*, **1996**, *3*, 147.
- 12 (32) Ankudinov, A. I.; Ravel, B.; Rehr, J. J.; Conradson, S. D. *Phys. Rev. B.* **1998**, *58*, 7565.
- 13 (33) Lee, P. A.; Citrin, P. H.; Eisenberger, P.; Kincaid, B. M. *Rev. Mod. Phys.* **1981**, *53*, 769.
- 14 (34) James, F. *CERN Program Library*, **1994**, 506.
- 15 (35) Kresse, G.; Hafner, J. *Phys. Rev. B.* **1993**, *47*, 558; Kresse, G.; Hafner, J. *Phys. Rev. B.*
16 **1994**, *49*, 14251.; Kresse, G.; Furthmüller, J. *Comput Mat. Sci.* **1996**, *6*, 15; Kresse, G.;
17 Furthmüller, J. *Phys Rev. B.* **1996**, *54*, 11169.
- 18 (36) Kresse, G.; Joubert, D. *Phys. Rev. B.* **1999**, *59*, 1758.
- 19 (37) Mihalkovic, M.; Widom, M. *Phys. Rev. B.* **2004**, *70*, 144107.
- 20 (38) Mulliken, R. S. *J. Chem. Phys.* **1955**, *23*, 1833.
- 21 (39) Sánchez-Portal, D.; Artacho, E.; Soler, J. M.; *Sol. St. Comm.* **1995**, *95*, 685.
- 22 (40) Segall, M. D.; Pickard, C. J.; Shah, R.; Payne, M. C.; *Mol. Phys.* **1996**, *89*, 571.
- 23 (41) Segall, M. D.; Shah, R.; Pickard, C. J.; Payne, M. C.; *Phys. Rev. B.* **1996**, *54*, 16317.
- 24 (42) Winkler, B.; Pickard, C. J.; Segall, M. D.; Milman, V. *Phys. Rev. B.* **2001**, *63*, 214103

- 1 (43) Clark, S. J.; Segall, M. D.; Pickard, C. J.; Hasnip, P. J.; Probert, M. J.; Refson, K.; Payne
2 M. C. *Zeits. Krist.* **2005**, *220*, 567.
- 3 (44) Perdew, J. P.; Burke, K.; Ernzerhof, M. *Phys. Rev. Lett.*, **1996**, *77*, 3865.; Perdew, J. P.;
4 Burke, K.; Ernzerhof, M. *Phys. Rev. Lett.*, **1997**, *78*, 1396.
- 5 (45) Kresse, G.; Hafner, J. *J. Phys.: Condens. Matter*, **1994**, *6*, 8245.
- 6 (46) *Inorganic Crystal Structure Database (ICSD)*. [<http://icsd.ill.fr/icsd/>].
- 7 (47) Pourbaix, M. *Atlas of Electrochemical Equilibria in Aqueous Solutions*. Pergamon Press,
8 1974.
- 9 (48) Kolitsch, U. *Acta Cryst. C*. **2004**, *60*, i94-i96.
- 10 (49) Loureiro, S. M.; Radaelli, P. G.; Antipoc, E. V.; Capponi, J. J.; Souletie, B.; Brunner, M.;
11 Marezio, M. *J. Sol. St. Chem.* **1996**, *121*, 66.

Table 1. Description of the samples with the initial concentration of As(V) in solution and total concentration of As(V) in the solids (adsorbed and substituted) as measured by ICP-AES. Speciation data have been taken from Pourbaix [46].

Sample label	pH	Predominant As species	Initial [As(V)] in solution (M)	[As(V)] in solids (mM/kg)
Y0	7.5	~50% H_2AsO_4^- ~50% HAsO_4^{2-}	0	0
Y1	4	H_2AsO_4^-	0.01	-
Y2	4		0.04	121
Y3	4		0.06	60.28
Y4	4		0.09	371
Y5	7.5	~50% H_2AsO_4^- ~50% HAsO_4^{2-}	0.01	82
Y6	7.5		0.04	219
Y7	7.5		0.06	975
Y8	7.5		0.09	799
Y9	9	HAsO_4^{2-}	0.01	105
Y10	9		0.04	548
Y11	9		0.06	789

1 **Table 2.** Atomic positions in unit cell for pure gypsum. Atomic positions from [29]† and [30]‡ are
 2 given in *italic* for the sake of comparison.

Atom	X	Y	Z	$U_{\text{iso}} (\text{Å}^2)$
Ca	0.5	0.0800(4)	0.25	0.0034(6)
	<i>†</i> 0.5	<i>†</i> 0.07960(4)	<i>†</i> 0.25	<i>†</i> 0.0095(2)
	<i>‡</i> 0.5	<i>‡</i> 0.0786(3)	<i>‡</i> 0.25	<i>‡</i> 0.0072
S	0.0	0.0774(5)	0.75	0.0021(7)
	<i>†</i> 0.0	<i>†</i> 0.07758(6)	<i>†</i> 0.75	<i>†</i> 0.0101(3)
	<i>‡</i> 0.0	<i>‡</i> 0.0787(4)	<i>‡</i> 0.75	<i>‡</i> 0.0064
O(1)	0.963(1)	0.1333(5)	0.550(1)	0.0104(9)
	<i>†</i> 0.9631(2)	<i>†</i> 0.1317(1)	<i>†</i> 0.5478(2)	<i>†</i> 0.0088(4)
	<i>‡</i> 0.9616(5)	<i>‡</i> 0.1326(1)	<i>‡</i> 0.5512(4)	<i>‡</i> 0.0149
O(2)	0.759(1)	0.0217(5)	0.666(1)	0.0085(9)
	<i>†</i> 0.7559(2)	<i>†</i> 0.0216(1)	<i>†</i> 0.6631(2)	<i>†</i> 0.0092(4)
	<i>‡</i> 0.7571(5)	<i>‡</i> 0.0215(2)	<i>‡</i> 0.6653(4)	<i>‡</i> 0.0123
O(3)	0.375(1)	0.1833(5)	0.457(1)	0.0133(9)
	<i>†</i> 0.3796(3)	<i>†</i> 0.1822(1)	<i>†</i> 0.4592(2)	<i>†</i> 0.0151(4)
	<i>‡</i> 0.3784(6)	<i>‡</i> 0.1826(2)	<i>‡</i> 0.4564(5)	<i>‡</i> 0.0222
H(1)	0.247(3)	0.165(1)	0.509(3)	0.020(2)
	<i>†</i> 0.250(3)	<i>†</i> 0.1536(7)	<i>†</i> 0.482(3)	<i>†</i> 0.085(6)
	<i>‡</i> 0.2504(6)	<i>‡</i> 0.1615(2)	<i>‡</i> 0.5009(6)	<i>‡</i> 0.0446
H(2)	0.399(3)	0.242(1)	0.491(3)	0.022(2)
	<i>†</i> 0.409(4)	<i>†</i> 0.2412(5)	<i>†</i> 0.500(4)	<i>†</i> 0.085(6)
	<i>‡</i> 0.4023(7)	<i>‡</i> 0.2435(2)	<i>‡</i> 0.4900(6)	<i>‡</i> 0.0389

3

1 **Table 3.** Unit cell parameters from combined refinement of neutron and X-ray data together with
 2 parameters related to the goodness of refinements R-Bragg and χ^2 for neutrons (RB_n , χ^2_n) and X-ray
 3 ($RB_{x\text{-ray}}$, $\chi^2_{x\text{-ray}}$).

pH	[As(V)] (M)	a (Å)	b (Å)	c (Å)	β (°)	Vol unit cell (Å ³)	RB_n	χ^2_n	$RB_{x\text{-ray}}$	$\chi^2_{x\text{-ray}}$
7.5	0.00	5.6929 (6)	15.245 (2)	6.5440 (4)	118.480 (4)	499.26 (2)	3.00	10.2	5.2	2.5
4	0.01	5.6923 (7)	15.245 (5)	6.5439 (4)	118.483 (1)	499.12 (1)	3.49	30	14.9	4.60
	0.04	5.6922 (1)	15.246 (4)	6.5429 (3)	118.480 (4)	499.08 (2)	7.45	60	12.3	4.03
	0.06	5.6923 (5)	15.246 (7)	6.5431 (8)	118.483 (5)	499.11 (2)	9.40	38.9	9.32	2.75
	0.09	5.6929 (2)	15.247 (1)	6.5436 (5)	118.479 (2)	499.24 (2)	9.21	46.6	16.9	4.23
7.5	0.01	5.6949 (5)	15.254 (9)	6.5406 (6)	118.441 (2)	499.61 (2)	4.54	27.6	11.4	3.48
	0.04	5.6956 (4)	15.258 (8)	6.5391 (7)	118.339 (6)	499.73 (6)	4.79	31.3	8.88	3.40
	0.06	5.6942 (3)	15.256 (6)	6.5389 (3)	118.432 (5)	499.52 (4)	4.30	32	9.88	3.83
	0.09	5.6955 (4)	15.259 (5)	6.5379 (7)	118.411 (4)	499.76 (7)	9.23	80.7	15.2	5.83
9	0.01	5.6973 (7)	15.264 (8)	6.5364 (2)	118.388 (3)	500.09 (2)	3.61	21	8.32	2.95
	0.04	5.7011 (8)	15.270 (8)	6.5329 (5)	118.427 (5)	500.57 (5)	7.18	31.9	28.4	3.73
	0.06	5.7010 (8)	15.272 (4)	6.5468 (9)	118.431 (7)	501.27 (8)	9.20	64.9	40.3	5.79

1 **Table 4.** Bond-lengths and Debye-Waller factors of the EXAFS analyses of the samples Y6, Y8 and
 2 Y11 and bond-lengths of the theoretical model obtained with the *ab-initio* calculations.

3 * Path-lengths of the first shell single scattering path for each of the two different ions: AsO_4^{3-} and
 4 HAsO_4^{2-} .

Y6			
Path	N	R (Å)	σ^2 (Å²)
As-O	4	1.68 ± 0.03	0.002 ± 0.003
As-Ca ₁	1	3.16 ± 0.05	0.001 ± 0.004
As-Ca ₂	1	3.31 ± 0.03	0.001 ± 0.004
As-Ca ₃	1	3.71 ± 0.06	0.001 ± 0.004
Y8			
Shell	N	R (Å)	σ^2 (Å²)
As-O	4	1.67 ± 0.03	0.001 ± 0.003
As-Ca ₁	1	3.14 ± 0.05	0.004 ± 0.005
As-Ca ₂	1	3.22 ± 0.07	0.004 ± 0.005
As-Ca ₃	1	3.70 ± 0.06	0.004 ± 0.005
Y11			
Shell	N	R (Å)	σ^2 (Å²)
As-O	4	1.68 ± 0.01	0.002 ± 0.001
As-Ca ₁	1	3.18 ± 0.05	0.003 ± 0.004
As-Ca ₂	1	3.30 ± 0.08	0.003 ± 0.004
As-Ca ₃	1	3.70 ± 0.07	0.003 ± 0.004
Theoretical model: HAsO_4^{2-} in gypsum			
Shell	N	R (Å)	
As-O	4	(1.69) (1.69, 1.79)*	
As-Ca ₁	1	3.10	
As-Ca ₂	1	3.31	
As-Ca ₃	1	3.70	
Theoretical model: pure gypsum			
S-O	4	1.48	
S-Ca _{1,2}	2	3.12	
S-Ca _{3,4}	2	3.70	

1 **Table 5.** Mulliken charges and effective ionic valences for the three models of pure and doped gypsum.
 2 The spilling parameter for each of the calculations is also presented. The labels of the atoms are
 3 explained on Figure 7. Both the Mulliken charges and the effective ionic valence values are given in e^- .

Material	Ion	Atom	Mulliken charge	Effective ionic valence
Gypsum	SO_4^{2-}		-1.38	0.62
		S	2.38	
		$\text{O}_{1,2}$	-0.95	
		$\text{O}_{3,4}$	-0.93	
	$\text{Ca}_{1,2,3,4}^{2+}$		1.42	0.58
Spilling parameter $s_1 = 1.3 \times 10^{-2}$				
HAsO ₄ doped gypsum	HAsO_4^{2-}		-1.37	0.63
		As	2.25	
		$\text{O}_{1,2}$	-0.90	
		O_3	-0.88	
		O_4	-0.94	
		H	0.44	
	$\text{Ca}_{1,2}^{2+}$		1.37	0.63
	Ca_3^{2+}		1.39	0.61
Ca_4^{2+}		1.41	0.59	
Spilling parameter $s_2 = 1.2 \times 10^{-2}$				
AsO ₄ doped gypsum	AsO_4^{3-}		-1.29	1.71
		As	2.24	
		$\text{O}_{1,2}$	-0.89	
		O_3	-0.87	
		O_4	-0.88	
	$\text{Ca}_{1,2}^{2+}$		1.30	0.70
	$\text{Ca}_{3,4}^{2+}$		1.37	0.63
Spilling parameter $s_3 = 1.1 \times 10^{-2}$				

4

1 **Table 6.** Bond lengths (given in Å) and bond populations (given in $e^- \text{Å}^{-3}$). A negative number in the
 2 bond population means the character of the bond is antibonding. $\langle x \rangle$ stands for the mean value. The
 3 labels of the atoms are explained on Figure 7.

SO42-			HAsO42-			AsO42-		
Atoms	Bond length	Bond population	Atoms	Bond length	Bond population	Atoms	Bond length	Bond population
Ca-S	3.12	-0.20	Ca-As	3.08	-0.35	Ca-As	3.15	-0.73
Ca1-O1	2.53	0.06	Ca1-O1	2.47	0.08	Ca1-O1	2.56	0.06
Ca1-O3	2.52	0.06	Ca1-O3	2.60	0.03	Ca1-O3	2.42	0.10
Ca2-O2	2.53	0.06	Ca2-O2	2.56	0.06	Ca2-O2	2.56	0.06
Ca2-O4	2.52	0.06	Ca2-O4	2.43	0.08	Ca2-O4	2.42	0.10
Ca3-O3	2.35	0.09	Ca3-O3	2.41	0.05	Ca4-O3	2.28	0.12
Ca4-O4	2.35	0.09	Ca4-O4	2.56	0.06	Ca3-O4	2.28	0.12
$\langle \text{Ca-O} \rangle$	2.47	0.07	$\langle \text{Ca-O} \rangle$	2.45	0.07	$\langle \text{Ca-O} \rangle$	2.42	0.10

1 **Table 7.** Concentration of arsenic incorporated into the bulk of gypsum. The values have been obtained
2 by interpolating the experimental volume expansion data in the theoretical volume expansion curves.

Initial [As] in solution (M)	pH 4	pH 7.5	pH 9
	[As] (mM/kg)	[As] (mM/kg)	[As] (mM/kg)
0.01	0	62	145
0.04	0	84	232
0.06	0	46	355
0.09	0	89	-

3

1 **Figure 1.** Left: view of the gypsum crystallographic unit cell. Right: orthogonal views of the gypsum
2 unit cell with respect to the A crystallographic axis (up-left), C axis (up-right) and B axis (down-right).

3 **Figure 2.** X-ray diffraction patterns. Points: experimental data. Lines: best fit.

4 **Figure 3.** Neutron diffraction patterns. Points: experimental data. Lines: best fit.

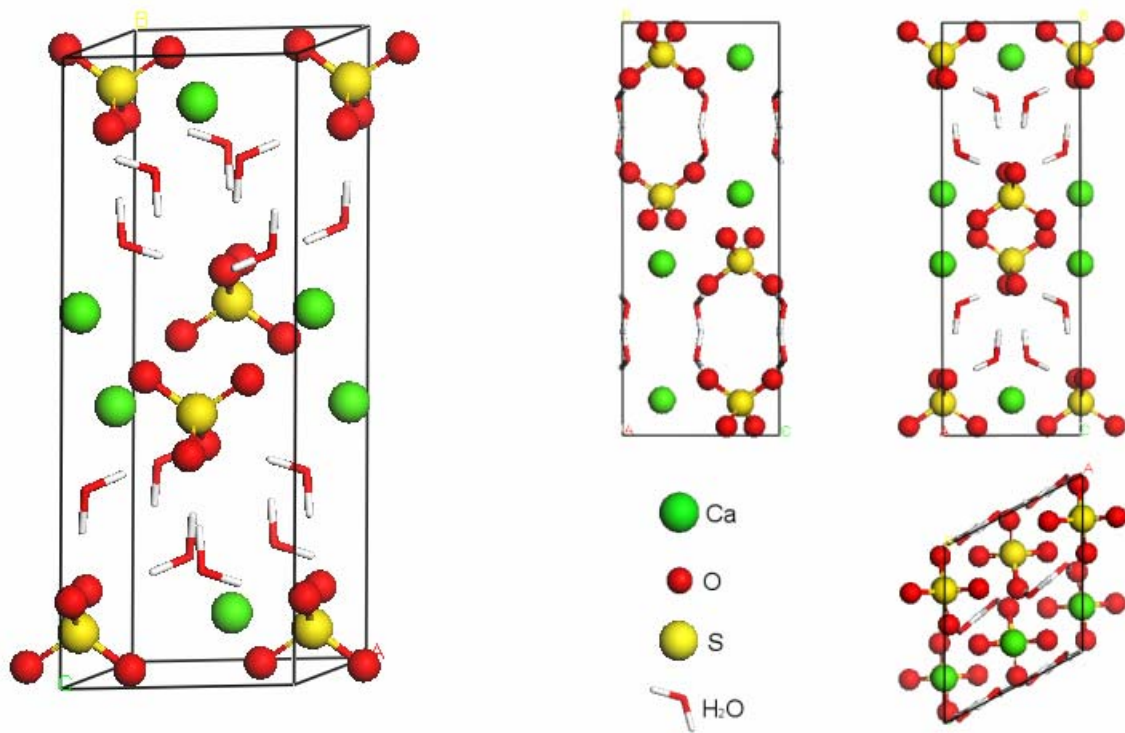
5 **Figure 4.** Unit cell volume for each of the samples. The common initial point for the three fit lines
6 corresponds to the structure of pure gypsum.

7 **Figure 5.** Simulated relative expansion of the unit cell volume of gypsum in function of the arsenic
8 concentration. The inset shows a detail of the interpolation of the experimental data using the simulated
9 expansion.

10 **Figure 6.** EXAFS signals and fit curves for the Y6, Y8, Y11 samples in the k space ($3.5-12 \text{ \AA}^{-1}$) and
11 their respective Fourier transforms (distances not corrected for phase shifts).

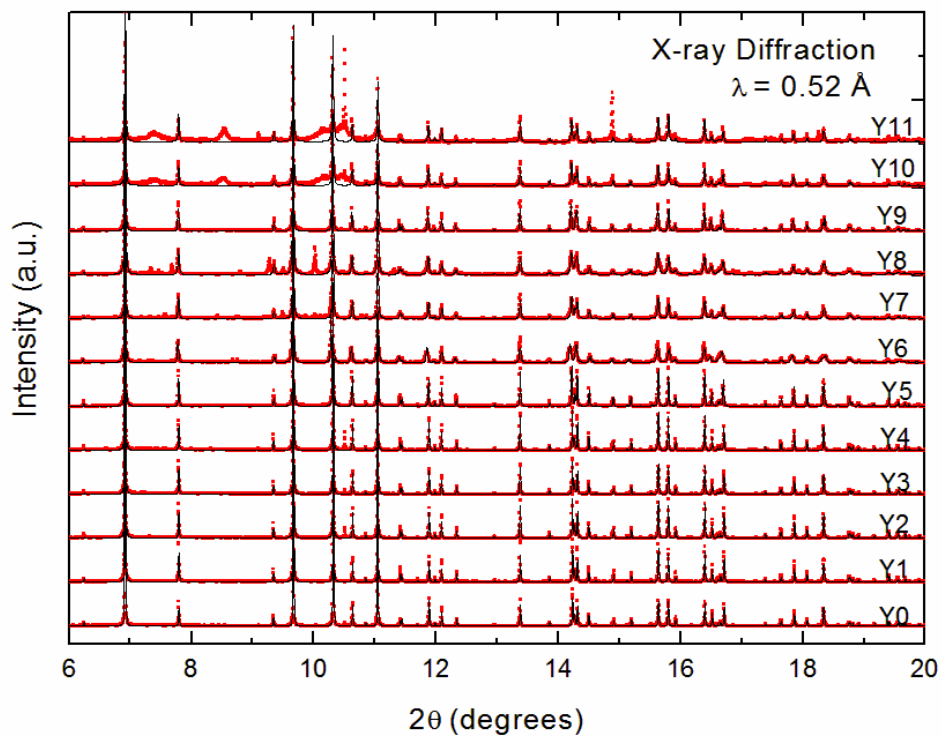
12 **Figure 7.** Atomistic models of the SO_4^{2-} , HAsO_4^{2-} and AsO_4^{3-} and their closer Ca shells within the
13 structure of gypsum. The dotted lines indicate the shorter Ca-O distances.

1 Figure 1.

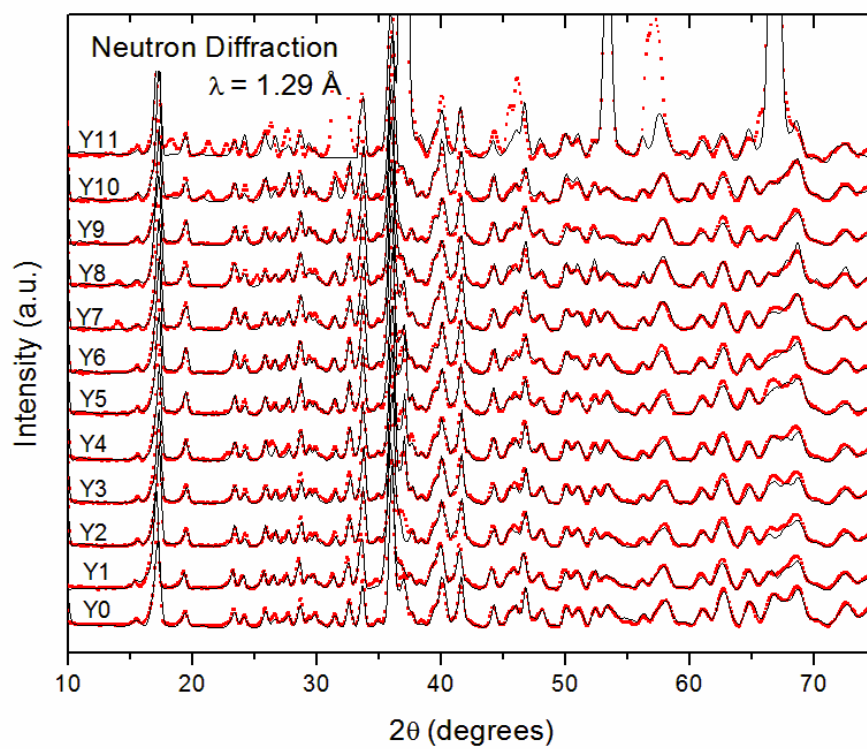


2

1 **Figure 2.**

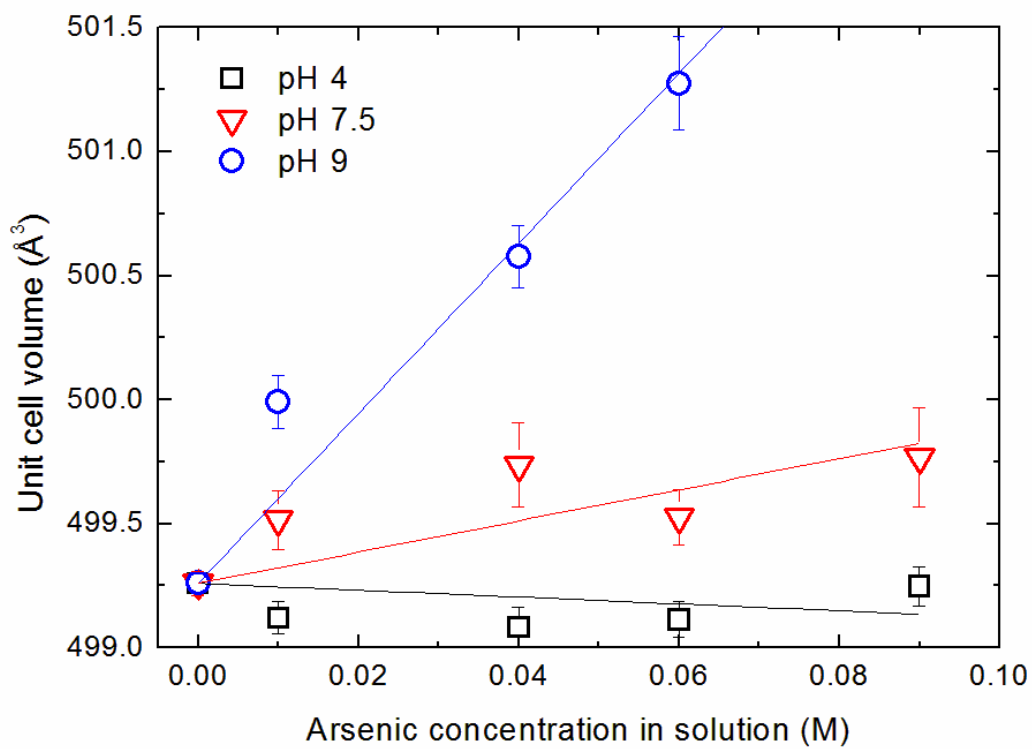


1 **Figure 3.**

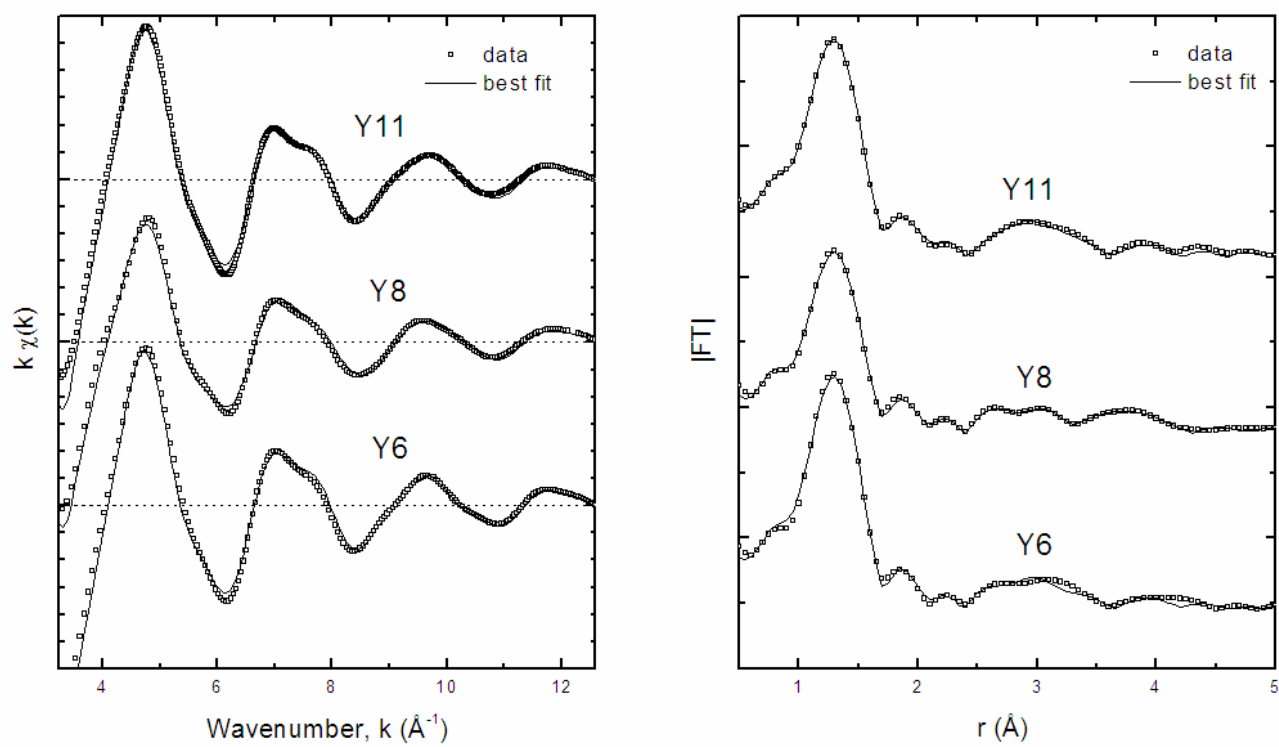


2

1 **Figure 4.**

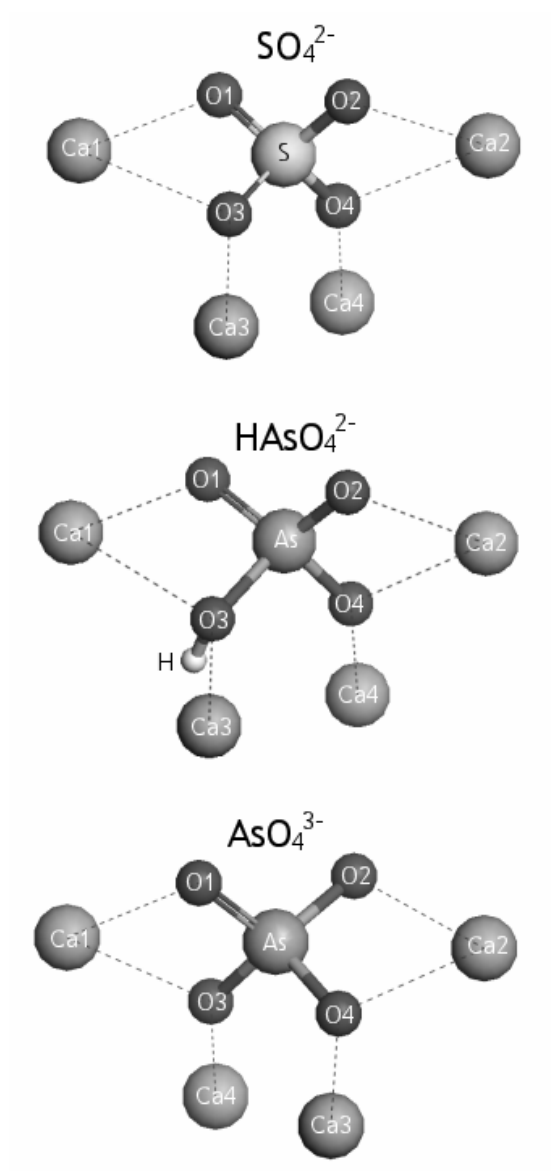


2

1 **Figure 6.**

2

1 **Figure 7.**



2